Dalton Transactions

ROYAL SOCIETY OF CHEMISTRY

Check for updates

Cu(II), Mn(II) and Zn(II) complexes of hydrazones with a quaternary ammonium moiety: synthesis, experimental and theoretical characterization and cytotoxic activity†

Nevena Stevanović,[a] Matija Zlatar, [iD][a] Irena Novaković,[b] Andrej Pevec,[a] Dušanka Radanović,[b] Ivana Z. Matić,[a] Marija Đorđić Crnogorac,[c] Tatjana Stanojković,[c] Miroslava Vujčić,[b] Maja Gruden, [iD][a] Dušan Sladić,[a] Katarina Anđelković,[a] Iztok Turel [iD] *[d] and Božidar Čobeljić [iD] *[a]

In this paper, Cu(II), Mn(II) and Zn(II) complexes with *N,N,N*-trimethyl-2-oxo-2-(2-(1-(thiazol-2-yl)ethyl-idene)hydrazinyl)ethan-1-aminium chloride (**HL**[1]**Cl**) were synthesized and characterized by single-crystal X-ray diffraction, IR spectroscopy, elemental analysis and DFT calculations. In all three complexes, a ligand (**L**[1]) is coordinated in a deprotonated formally neutral zwitterionic form *via* NNO donor set atoms. Cu(II) and Zn(II) form mononuclear penta-coordinated complexes [CuL[1](N$_3$)(CH$_3$OH)]BF$_4$ and [ZnL[1](N$_3$)$_2$], respectively, while Mn(II) forms a binuclear [Mn$_2$L[1]$_2$(μ-$_{1,1}$-N$_3$)$_2$(N$_3$)$_2$]·2CH$_3$OH complex, with unusual dis-torted trigonal-prismatic geometry around the metal centers. The antimicrobial activity of these com-plexes was tested against a panel of Gram-negative and Gram-positive bacteria, two yeasts and one fungal strain. The binuclear Mn(II) complex showed antifungal activity of similar intensity to amphotericin B. Based on the results of the brine shrimp test and DPPH radical scavenging activity, the most active Cu(II) and Mn(II) complexes were selected for evaluation of cytotoxic activity against five malignant cancer cell lines (HeLa, A375, MCF7, PC-3 and A549) and one normal cell line HaCaT. Both complexes showed significant activity. It should be pointed out that the activity of the Mn(II) complex against the MCF7 breast cancer cell line is only slightly weaker than that of cisplatin, but with selectivity to the tumor cell line in comparison to normal HaCaT cells, which is non-existent in the case of cisplatin.

Introduction

Metal complexes with hydrazones have been investigated intensively during previous years due to their various pharmaceutical applications as antitumor, antibacterial, antiviral and antifungal agents.[1] Of particular interest are hydrazone ligands with the –CH=N–NH–C(O)– group, formed by the condensation of aldehydes/ketones with different hydrazides. Girard's T reagent (trimethylaminoacetohydrazide chloride) is attractive due to its ability to form water-soluble hydrazones

with various aldehydes/ketones.[2] Using aldehydes/ketones with a thiazole ring in their structure for the synthesis of hydrazone ligands, additional coordination atoms are introduced. Combining both properties (additional coordination site due to the thiazole ring and water-solubility due to the positively charged quaternary ammonium moiety) in metal hydrazone complexes can lead to enhanced biological activity.[1]

Copper, manganese and zinc are essential trace elements with many physiological functions. Ions of these elements act as cofactors and as allosteric components for many enzymes.[3–5] Cu(II) and Mn(II) complexes have been studied as low molecular weight model compounds that mimic the active site of superoxide dismutase (SOD),[6,7] which participate in cell oxidative stress regulation. According to biological evaluations, complexes of Cu(II), Mn(II) and Zn(II) with Schiff base ligands can possess different biological activities, such as effective inhibition against bacteria[8–15] and fungi,[8,9,11,13,14] as well as cytotoxic activity.[8,16–18]

Schiff base complexes of Cu(II) and Mn(II), both mono-nuclear and dinuclear, were previously reported.[16,17,19] Most of

[a]University of Belgrade-Faculty of Chemistry, Studentski trg 12–16, 11000 Belgrade, Serbia. E-mail: bozidar@chem.bg.ac.rs
[b]University of Belgrade-Institute of Chemistry, Technology and Metallurgy, Department of Chemistry, Njegoševa 12, 11000 Belgrade, Serbia
[c]Institute of Oncology and Radiology of Serbia, 11000 Belgrade, Serbia
[d]Faculty of Chemistry and Chemical Technology, University of Ljubljana, Večna pot 113, 1000 Ljubljana, Slovenia. E-mail: Iztok.Turel@fkkt.uni-lj.si
†Electronic supplementary information (ESI) available. CCDC 2110386–2110388. For ESI and crystallographic data in CIF or other electronic format see DOI: 10.1039/d1dt03169d

the biologically active copper and manganese complexes have a mononuclear structure, with the most common being square-planar[17,18,20] and square-pyramidal geometry[8,16,18,21] around Cu(II) ions and octahedral geometry around Mn(II) ions.[13,22–24]

In continuation of our previous investigations on the synthesis, characterization and biological activity of complexes with Girard's T reagent-based hydrazones,[6,25–29] which showed moderate biological activities, in this paper, three novel Girard's T reagent–based complexes with Cu(II), Mn(II) and Zn(II) ions are described.

Results

General

The reaction of 2-acetylthiazole and Girard's T reagent was performed according to the previously reported method[30] which yielded the ligand N,N,N-trimethyl-2-oxo-2-(2-(1-(thiazol-2-yl) ethylidene)hydrazinyl)ethan-1-aminium chloride (**HL^{1}Cl**) that was used for the synthesis of complexes **1–3** (Scheme 1). The reaction of the ligand **HL^{1}Cl** with the metal salts Cu(BF$_4$)·6H$_2$O/MnCl$_2$·4H$_2$O/Zn(BF$_4$)·6H$_2$O and NaN$_3$ in the molar ratio 1 : 1 : 4 in methanol results in the formation of mononuclear Cu(II) complex (**1**) with the composition [CuL^1(N$_3$)(CH$_3$OH)]BF$_4$, binuclear Mn(II) complex **2** with the composition [Mn$_2$L$^1_2$(μ$_{-1,1}$-N$_3$)$_2$(N$_3$)$_2$]·2CH$_3$OH, and mono-

nuclear Zn(II) complex (**3**) with the composition [ZnL^1(N$_3$)$_2$] (Scheme 1). The ligand is coordinated in a deprotonated formally neutral zwitterionic form via NNO donor set atoms in all three complexes.

Spectroscopy

IR spectra. The IR spectroscopy data confirm that the **HL^{1}Cl** ligand (Fig. S4†) is coordinated in a deprotonated form as the ν(N–H) band at 2955 cm^{-1} is absent in the spectrum of all complexes.[31] The presence of a medium sharp peak at 3050 cm^{-1} in the spectrum of **1** (Fig. S5†) and a medium broad peak at 3388 cm^{-1} in the spectrum of **2** (Fig. S6†) point to the coordination of methanol ν(O–H) in the case of complex **1** and the presence of methanol in the crystals of complex **2**. In the IR spectra, strong bands at 2047 cm^{-1}, 2042 cm^{-1} and 2057 cm^{-1} originate from coordinated N$_3^-$ for complexes **1**, **2** and **3** (Fig. S7 and S8†), respectively. In the case of complex **2**, an additional weak band at 2111 cm^{-1} is assigned to the bridging azido ligand. Instead of the ν(C=O) band at 1701 cm^{-1}, observed in the spectrum of the ligand **HL^{1}Cl**, new bands at 1698 cm^{-1}, 1688 cm^{-1} and 1690 cm^{-1} appeared in the spectra of complexes **1**, **2** and **3**, respectively, assigned to the ν(–O–C=N) vibrations of the deprotonated hydrazide moieties. The coordination of azomethine nitrogen atoms results in the shift of the ν(C=N) band from 1612 cm^{-1} in the spectrum of the ligand **HL^{1}Cl** to 1604 cm^{-1}, 1595 cm^{-1}, and 1600 cm^{-1} in the spectra of complexes **1**, **2** and **3**, respectively.
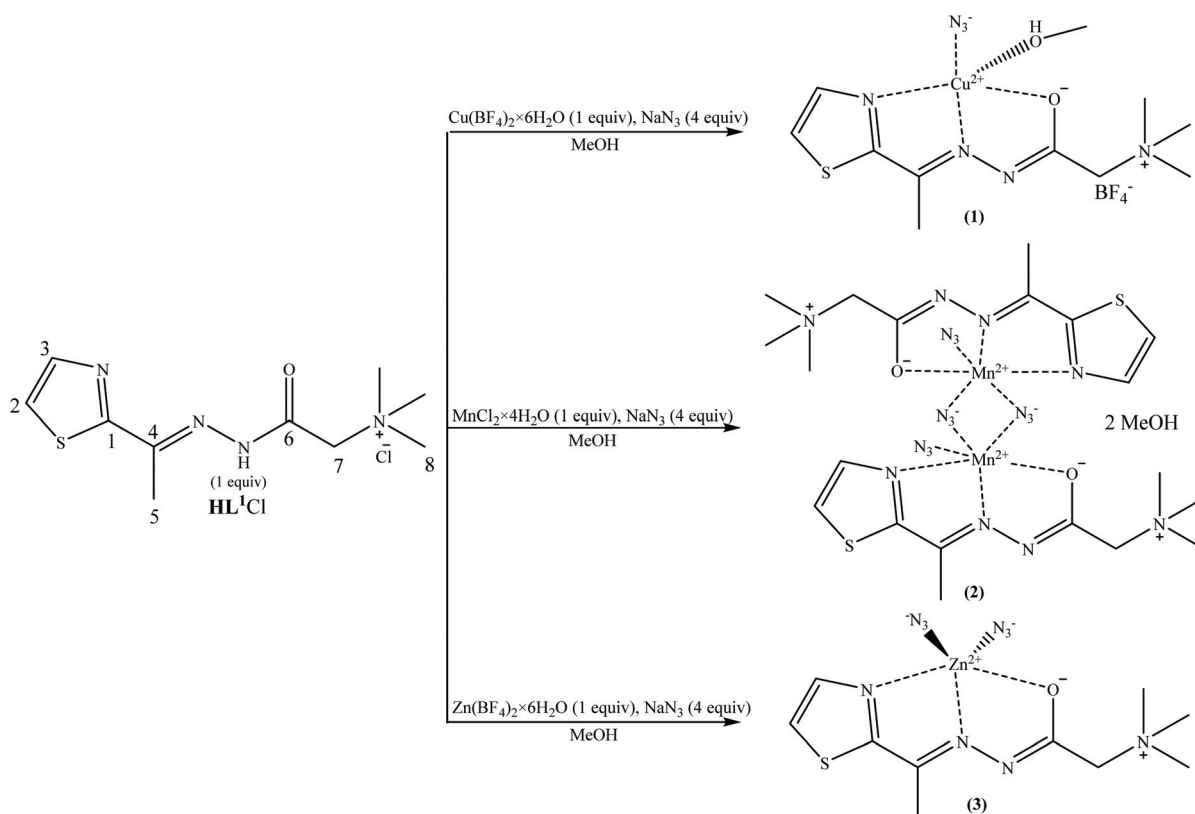
Scheme 1 Synthesis of the [CuL^1(N$_3$)(CH$_3$OH)]BF$_4$ (**1**), [Mn$_2$L$^1_2$(μ$_{-1,1}$-N$_3$)$_2$(N$_3$)$_2$]·2CH$_3$OH (**2**) and [ZnL^1(N$_3$)$_2$] (**3**) complexes.

NMR spectra. The signal of hydrazide NH at 11.86 ppm (Fig. S9†) is absent in the ^{1}H NMR spectrum of complex **3** (Fig. S10†), indicating that the ligand is coordinated in a deprotonated zwitterionic form. Coordination of thiazole nitrogen in the Zn(II) complex can be confirmed from a downfield shift of C3–H from 7.93 ppm in the spectrum of **HL**[1]**Cl** to 8.04 ppm in the spectrum of the Zn(II) complex. Due to the carbonyl oxygen atom's coordination, the carbonyl carbon (C6) signal is shifted downfield from 167.04 ppm in the spectrum of **HL**[1]**Cl** (Fig. S11†) to 171.59 ppm in the spectrum of complex **3** (Fig. S12†). The downfield shift of the azomethine carbon atom (C4) signal from 146.98 ppm in the spectrum of **HL**[1]**Cl** to 147.32 ppm in the spectrum of the Zn(II) complex indicates the coordination of the azomethine nitrogen. The coordination of the thiazole nitrogen atom caused an upfield shift of the C3 atom signal from 143.94 ppm in the spectrum of **HL**[1]**Cl** to 143.44 ppm in the spectrum of the Zn(II) complex.

Crystal structures of [CuL[1](N₃)(CH₃OH)]BF₄ (1), [Mn₂L[1]₂(μ₋₁,₁-N₃)₂(N₃)₂]·2CH₃OH (2) and [ZnL[1](N₃)₂] (3) complexes

The Cu(II), Mn(II) and Zn(II) ions with **L**[1] form the mononuclear [CuL[1](N₃)(CH₃OH)]BF₄ (**1**) and [ZnL[1](N₃)₂] (**3**) and binuclear [Mn₂L[1]₂(μ₋₁,₁-N₃)₂(N₃)₂]·2CH₃OH (**2**) complexes in which **L**[1] in a zwitterionic form[2] coordinates as a tridentate ligand to M(II) ions through thiazole and imine nitrogen atoms and an enolate oxygen atom. Complexes **1** and **3** crystallize in the monoclinic crystal system with space group No. 14 ($P2_1/n$ and $P2_1/c$ cell settings, respectively) and complex **2** in the triclinic crystal system with the space group $P\bar{1}$ (No. 2).

Crystal structure of complex 1. The asymmetric unit (asu) of **1** consists of a complex cation [CuL[1](N₃)(CH₃OH)]⁺ and a BF₄⁻ anion. The molecular structure of the complex cation [CuL[1](N₃)(CH₃OH)]⁺ with the atom numbering scheme is shown in Fig. 1. Selected bond distances and valence angles are given in Table S1.† The Cu(II) ion has a fivefold coordination with the in-plane coordinated **L**[1] through the NNO-set of donor atoms and one nitrogen atom (N5) of the azide

ligand, while the apical position is occupied by an oxygen atom (O2) from methanol. In general, the distortion in the five-coordinated systems is described by an index of trigonality $\tau = (\beta - \alpha)/60$, where β is the greatest basal angle and α is the second greatest angle.[32] The parameter τ is 0 for regular square-based pyramidal forms and 1 for trigonal bipyramidal forms. The five-coordination geometry of the Cu(II) ion can be described as distorted square-based pyramidal, as indicated by the τ value of 0.26. The greatest basal angles N5–Cu1–N2 and O1–Cu1–N1 are 174.8(1)° and 159.05(9)°, respectively. The Cu(II) ion is shifted by 0.1038(4) Å from the basal plane towards the apical ligand atom (O2). The dihedral angle of nearly 5.0° between two five-membered chelate rings (Cu–N–C–C–N and Cu–N–N–C–O) shows the non-coplanar nature of the metal–ligand system in **1**. The Cu–N$_{Ar}$, Cu–N$_{imine}$ and Cu–O$_{enolate}$ bond lengths of 2.048(2) Å, 1.928(2) Å and 1.970(2) Å in **1** are comparable with those observed in the structurally related [CuL[2]Cl(BF₄)], [CuL[2]Cl(NO₃)] and [CuL[2]Cl(ClO₄)] complexes (**L**[2] = the condensation product of 2-acetylpyridine and tri-methylammoniumacetohydrazide chloride) of distorted square pyramidal geometry in which the apical ligands BF₄⁻, NO₃⁻, and ClO₄⁻ are weakly coordinatively bound to Cu(II) ions.[33,34] The axial Cu1–O2 2.533(2) Å bond in **1** is shorter than the Cu⋯F(BF₄⁻) 2.581(4) Å, Cu⋯O(NO₃⁻) 2.607(2) Å and Cu⋯O (ClO₄⁻) 2.73(1) Å axial bonds in [CuL[2]Cl(BF₄)],[35] [CuL[2]Cl (NO₃)][35] and [CuL[2]Cl(ClO₄)][34,35] complexes, respectively. In the crystals of **1**, complex cations form hydrogen-bonded dimers at $\frac{1}{2}$ $\frac{1}{2}$ 0 and 0 0 $\frac{1}{2}$ through intermolecular O2–H2A⋯N5 hydrogen bonds (Table S4 and Fig. S1†). The counter anion (BF₄⁻) mediates in joining the H-bonded dimers into layers parallel to the (202) lattice plane through intermolecular C–H⋯F hydrogen bonds (Table S4 and Fig. S1a†) and assists in connecting the neighboring layers by means of C–H⋯F hydrogen bonds (Table S4 and Fig. S1b†). The Cu1⋯Cu1^a (a = 1 − x, 1 − y, −z) separation of 4.9983(7) Å observed in the H-bonded dimers is greater than those found in the pseudo-dimeric structures of the [CuL[2]Cl(BF₄)], [CuL[2]Cl(NO₃)] and [CuL[2]Cl(ClO₄)] complexes (3.5793–3.7973 Å).[34,35] However, in the crystal structure of **1**, the shortest Cu⋯Cu^b (b = −x, 1 − y, −z) separation of 3.384 Å has been observed between the Cu(II) ions belonging to the neighboring (202) layers (Fig. S1b†).

Crystal structure of complex 2. The crystal structure of **2** displays a centrosymmetric binuclear complex with the asymmetric unit comprising one Mn(II) center, one ligand **L**[1], two azide anions (one bridging and one terminal) and one solvent (methanol) molecule. The molecular structure of [Mn₂L[1]₂(μ₋₁,₁-N₃)₂(N₃)₂] with the atom numbering scheme is shown in Fig. 2. Selected bond distances and valence angles are given in Table S2.† The Mn(II) ion is hexacoordinated with three donor atoms N1, N2 and O1 of ligand **L**[1], two nitrogen atoms (N5 and N5^c where c is 1 − x, 1 − y, 1 − z) from the bridging azide anions, and one nitrogen atom (N8) from the terminal azide anion. The polyhedron around the Mn(II) ion is described as a distorted trigonal prism (TPR-6) with a twist angle Φ of 14.19° (mean value) being calculated by applying method 1 reported in ref. 36 for the atom pairs N1N8, O1N2 and N5N5^c.
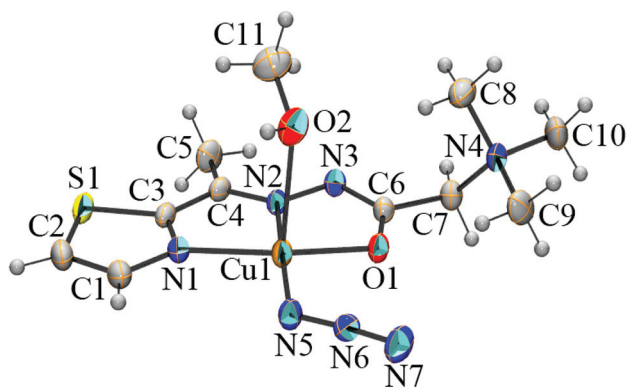

Fig. 1 ORTEP representation of the [Cu(L[1])(N₃)(CH₃OH)]⁺ complex cation in [CuL[1](N₃)(CH₃OH)]BF₄. Thermal ellipsoids are drawn at the 30% probability level.
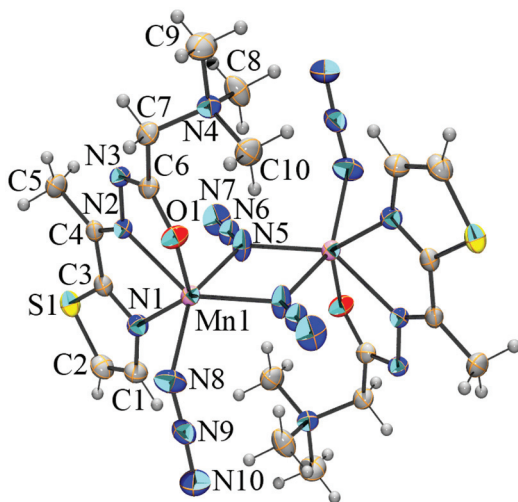
Fig. 2 ORTEP representation of [Mn$_2$**L**$^1_2$(μ-$_{1,1}$-N$_3$)$_2$(N$_3$)$_2$] in [Mn$_2$**L**$^1_2$(μ-$_{1,1}$-N$_3$)$_2$(N$_3$)$_2$]·2CH$_3$OH. The unlabelled part of the molecule is generated by symmetry operation 1 − x, 1 − y, and 1 − z. Solvent CH$_3$OH molecules have been omitted for clarity. Thermal ellipsoids are drawn at the 30% probability level.

Comparing with the octahedral Ni(II) complexes [Ni$_2$**L**$^1_2$(μ-$_{1,1}$-N$_3$)$_2$(N$_3$)$_2$]·2H$_2$O and [Ni$_2$**L**$^1_2$(μ-$_{1,1}$-N$_3$)$_2$(N$_3$)$_2$]·4H$_2$O [37] with the same ligand, the [Mn$_2$**L**$^1_2$(μ-$_{1,1}$-N$_3$)$_2$(N$_3$)$_2$]·2CH$_3$OH (**2**) complex shows significantly longer M–N$_{Ar}$ and M–N$_{imine}$ bond distances (Mn–N$_{Ar}$ 2.3668(19) Å, Ni–N$_{Ar}$ 2.122(2)–2.126(3) Å; Mn–N$_{imine}$ 2.2500(18) Å, Ni–N$_{imine}$ 1.997(2)–2.017(3) Å; Mn–O$_{enolate}$ 2.1879 (16) Å and Ni–O$_{enolate}$ 2.083(2)–2.140(2) Å), indicating the weaker coordination of **L**^{1} to Mn(II) ions. Similarly, as in the corresponding Ni(II) complexes,[37] in complex **2**, the terminal azido ligands are coordinated at *trans* positions. The N9–N8–Mn1 bond angle of 137.7(2)° shows the bent coordination of the anionic terminals. The central Mn$_2$N$_2$ ring is planar with a Mn–N$_{azido(end-on)}$–Mn^c bridging angle of 107.37(8)° and an Mn···Mn^c separation of 3.6031(6) Å. The Mn–N$_{azido(end-on)}$ bond distances show a discrepancy of 0.0135 Å. In the crystals of **2**, binuclear complex units are connected by weak intermolecular C–H···O$_{enolate}$ and C–H···N$_{azide}$ hydrogen bonds[38] into chains parallel with [100]. Furthermore, the chains are connected by intermolecular hydrogen bonds that involve solvent methanol molecules serving as hydrogen bond donors (O2–H2A···N3) and hydrogen bond acceptors (C7–H7B···O2 and C9–H9C···O2) into layers parallel with the (0−11) lattice plane (Table S5 and Fig. S2†). The shortest separation of 4.6162(16) Å between the centers of gravity of the 1,3-thiazole rings is observed between the neighboring (0−11) layers.

Crystal structure of complex 3. The asymmetric unit of **3** consists of the neutral [Zn**L**^{1}(N$_3$)$_2$] complex. The molecular structure of [Zn**L**^{1}(N$_3$)$_2$] with the atom numbering scheme is shown in Fig. 3. Selected bond distances and valence angles are given in Table S3.† In the [Zn**L**^{1}(N$_3$)$_2$] complex, the Zn(II) ion has fivefold coordination with the NNO-set of donor atoms of **L**^{1} and two nitrogen atoms (N5 and N8) from the azido ligands. The calculated τ value of 0.43 for [Zn**L**^{1}(N$_3$)$_2$] indicates
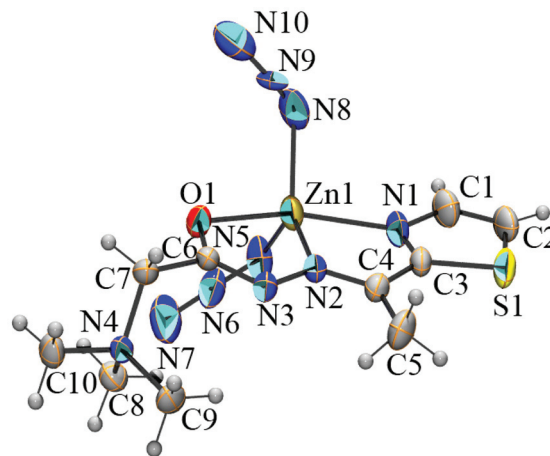

Fig. 3 ORTEP representation of the [Zn**L**^{1}(N$_3$)$_2$] complex. Thermal ellipsoids are drawn at the 30% probability level.

that the five-coordination geometry of the Zn(II) ion is almost midway between the square-based pyramidal and trigonal bipyramidal forms. The greatest basal angles N1–Zn1–O1 and N8–Zn1–N2 are 149.06(12)° and 123.30(18)°, respectively. In comparison with complex **3**, the other structurally related five-coordinate Zn(II) complexes containing heteroaromatic hydrazones of Girard's T reagent and monodentate ligands (N$_3^-$, NCO$^-$, NCS$^-$ or Cl$^-$) exhibit a somewhat smaller degree of trigonal distortion from the ideal square-based pyramidal configuration as indicated by the τ values that are in the range of 0.31–0.36 (ref. 30 and 39–41). The dihedral angle of nearly 4.0° between two five-membered chelate rings (Zn–N–C–C–N and Zn–N–N–C–O) shows the non-coplanar nature of the metal–ligand system in **3**. The Zn–N$_{Ar}$ 2.209(3) Å and Zn–N$_{imine}$ 2.064 (3) Å bond lengths observed in **3** fit into the range of values 2.206(6)–2.344(2) Å and 2.049(3)–2.088(6) Å, respectively, observed for the analogous Zn(II) complexes [Zn**L**^{1}(NCS)$_2$]·2H$_2$O,[27] [Zn**L**^{2}(NCS)$_2$]·0.5MeOH,[39] [Zn**L**^{3}(N$_3$)$_2$],[41] [Zn**L**^{3}(NCO)$_2$],[41] and [Zn**L**^{3}(N$_3$)$_{1.65}$Cl$_{0.35}$] [40] (**L**^{3} = the condensation product of 2-quinolinecarboxaldehyde and trimethylammoniumacetohydrazide chloride), while the Zn–O$_{enolate}$ bond is slightly longer—2.230(2) Å *vs.* 2.146(5)–2.222(2) Å. The azido ligands in **3** are coordinated to the Zn(II) ion in the bent mode, with Zn–N–N angles of 122.5(3) and 122.7(5)°. In the crystals of **3**, the complex molecules [Zn**L**^{1}(N$_3$)$_2$] are self-assembled into supramolecular layers parallel to the (100) lattice plane through weak intermolecular C–H···N and C–H···O hydrogen bonds[38] (Table S6 and Fig. S3†).

Computational results

DFT calculations were performed to elucidate the structures of the Cu(II), Mn(II), and Zn(II) complexes in DMSO solution. Free energy changes, Δ$_r$G (298 K), of several probable reactions starting from the X-ray determined structures of **1**, **2**, and **3** were investigated. There is an excellent agreement between the DFT optimized and X-ray structures for all three complexes (Fig. S13†). Δ$_r$G (298 K) was calculated based on the difference

in the Gibbs free energy of the products and reactants at the ZORA-M06-2X/TZP-COSMO(DMSO)//ZORA-BP86-D3/ TZP-COSMO(DMSO) level of theory. For the Cu(II) complex, we explored the formation of the binuclear complex $[Cu_2L^1_2(N_3)_2(CH_3OH)_2]^{2+}$, dissociation of weakly coordinated CH_3OH to form square-planar $[CuL^1(N_3)]^+$, and several potential modes of coordination of DMSO to the Cu(II) center (reactions (1)–(5), Table 1). The results clearly show that the formation of square planar $[CuL^1(N_3)]^+$ (Fig. 4) from **1** is thermodynamically favored. For the Mn(II) complex, we investigated the dissociation of crystalline CH_3OH from **2** and the dissociation of binuclear $[Mn_2L^1_2(\mu\text{-}_{1,1}\text{-}N_3)_2(N_3)_2]$ to form the mononuclear pentacoordinate complex $[MnL^1(N_3)_2]$ (reactions (6) and (7), Table 1). The subsequent formation of octahedral Mn(II) complexes with a solvent molecule (DMSO) as the sixth ligand is also considered (reactions (8) and (9), Table 1). The results reveal that the thermodynamically most favorable is the formation of the pentacoordinate $[MnL^1(N_3)_2]$ complex (Fig. 5). However, according to the calculated $\Delta_r G$ of only -1 kcal mol^{-1} for reaction (7), the binuclear $[Mn_2L^1_2(\mu\text{-}_{1,1}\text{-}N_3)_2(N_3)_2]$ complex is also expected to be present in the DMSO solution.

Fig. 5 Structure of the $[MnL^1(N_3)_2]$ complex optimized at the ZORA-BP86-D3/TZP-COSMO(DMSO) level of theory.

Table 1 Gibbs free energy changes ($\Delta_r G$ in kcal mol^{-1} at T = 298.15 K) calculated at the ZORA-M06-2X/TZP-COSMO(DMSO)//ZORA-BP86-D3/ TZP-COSMO(DMSO) level of theory for the formation of different Cu(II), Mn(II) and Zn(II) complexes starting from the X-ray determined structures of **1**, **2** and **3**

	Reaction	$\Delta_r G$ (298 K)
1	$2[CuL^1(N_3)(CH_3OH)]^+ \rightleftharpoons [Cu_2L^1_2(N_3)_2(CH_3OH)_2]^{2+}$	8.90
2	$[CuL^1(N_3)(CH_3OH)]^+ \rightleftharpoons [CuL^1(N_3)]^+ + CH_3OH$	−2.90
3	$[CuL^1(N_3)(CH_3OH)]^+ + DMSO \rightleftharpoons [CuL^1(N_3)(CH_3OH)(DMSO)]^+$	4.58
4	$[CuL^1(N_3)]^+ + DMSO \rightleftharpoons [CuL^1(N_3)(DMSO)]^+$	2.96
5	$[CuL^1(N_3)]^+ + 2DMSO \rightleftharpoons [CuL^1(N_3)(DMSO)_2]^+$	7.33
6	$[Mn_2L^1_2(\mu\text{-}_{1,1}\text{-}N_3)_2(N_3)_2]\cdot2CH_3OH \rightleftharpoons [Mn_2L^1_2(\mu\text{-}_{1,1}\text{-}N_3)_2(N_3)_2] + 2CH_3OH$	−9.93
7	$[Mn_2L^1_2(\mu\text{-}_{1,1}\text{-}N_3)_2(N_3)_2] \rightleftharpoons 2[MnL^1(N_3)_2]$	−1.07
8	$[MnL^1(N_3)_2] + DMSO \rightleftharpoons cis\text{-}[MnL^1(N_3)_2(DMSO)]$	2.96
9	$[MnL^1(N_3)_2] + DMSO \rightleftharpoons trans\text{-}[MnL^1(N_3)_2(DMSO)]$	2.47
10	$2[ZnL^1(N_3)_2] \rightleftharpoons [Zn_2L^1_2(\mu\text{-}_{1,1}\text{-}N_3)_2(N_3)_2]$	10.29
11	$[ZnL^1(N_3)_2] + DMSO \rightleftharpoons cis\text{-}[ZnL^1(N_3)_2(DMSO)]$	6.05
12	$[ZnL^1(N_3)_2] + DMSO \rightleftharpoons trans\text{-}[ZnL^1(N_3)_2(DMSO)]$	7.85

Two Mn(II) centers in $[Mn_2L^1_2(\mu\text{-}_{1,1}\text{-}N_3)_2(N_3)_2]$ are weakly ferromagnetically coupled, with the exchange constant J = 6.0 cm^{-1} calculated by the broken-symmetry DFT approach at the ZORA-M06-2X-COSMO(DMSO)/TZP level of theory. Analogous reactions were considered for the Zn(II) complex, *i.e.*, formation of the binuclear complex $[Zn_2L^1_2(\mu\text{-}_{1,1}\text{-}N_3)_2(N_3)_2]$ (reaction (10), Table 1) and the formation of six-coordinate complexes (reactions (11) and (12), Table 1). The calculations disclose that the $[ZnL^1(N_3)_2]$ complex (complex **3**) is thermodynamically preferred in DMSO solution.

Antimicrobial activity

The antibacterial activity of the synthesized complexes, their precursors HL^1Cl, NaN_3 and appropriate salts was evaluated against a panel of five Gram-positive and five Gram-negative bacteria. The MIC data are given in Table 2. All three complexes showed antibacterial activity against all tested bacterial strains. For complexes **1** and **2**, the precursor compounds either do not have or show low antibacterial activity. The most active complex **2** is also the only binuclear complex in the series. Its activity towards *P. aeruginosa* is over twice lower than the activity of chloramphenicol, while against *P. hauseri*, the activity was four times lower than the control compound. Complex **1** displayed the best activity towards *E. coli* strain and very weak selectivity towards Gram-negative bacteria. The lowest antibacterial activity was obtained for complex **3**. In some cases, its activity was lower than that of the parent salt. A comparison of the antimicrobial activity of binuclear azido bridged complexes of Mn(II) (complex **2**) and Ni(II) with the same ligand system[42] showed that complex **2** has higher antimicrobial activity. Even with this slightly lower activity, the

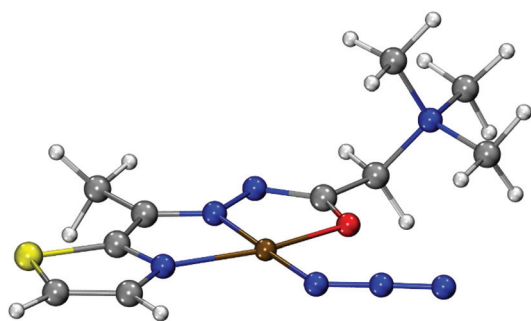**Fig. 4** Structure of the $[CuL^1(N_3)]^+$ complex ion optimized at the ZORA-BP86-D3/TZP-COSMO(DMSO) level of theory.

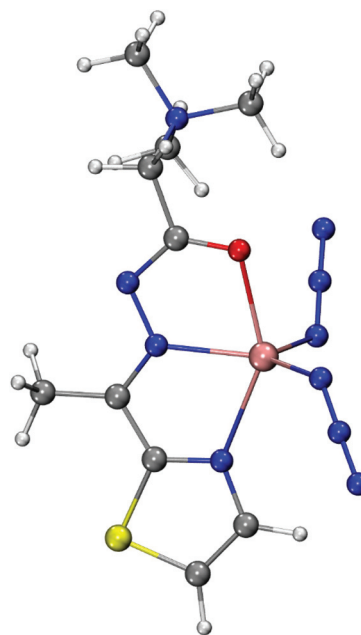**Table 2** Antibacterial activity (MIC in mM)

	E. coli	P. aeruginosa	P. hauseri	K. pneumoniae	S. enterica	S. aureus	M. flavus	M. luteus	B. spizizenii	C. sporogenes
HL^{1}Cl	—	—	—	—	—	—	—	—	—	—
1	1.19	2.37	4.74	2.37	2.37	4.74	4.74	4.74	4.74	4.74
2	1.44	1.44	1.44	1.44	1.44	2.88	1.44	1.44	1.44	2.88
3	2.75	2.75	5.50	2.75	2.75	2.75	2.75	2.75	5.50	5.50
[Ni$_2$L$^1_2$(μ-$_{1,1}$-N$_3$)$_2$(N$_3$)$_2$]·4H$_2$O (ref. 42)	1.56	3.12	3.12	3.12	1.56	3.12	1.56	1.56	3.12	3.12
Cu(BF$_4$)$_2$·6H$_2$O	7.33	7.33	7.33	7.33	7.33	7.33	7.33	7.33	7.33	7.33
MnCl$_2$·4H$_2$O	12.64	6.32	6.32	12.64	6.32	6.32	6.32	12.64	6.32	6.32
Zn(BF$_4$)$_2$·6H$_2$O	0.45	7.19	7.19	7.19	3.60	3.60	7.19	1.80	3.60	3.60
NaN$_3$	4.81	9.61	—	—	9.61	19.23	19.23	38.46	38.46	—
Chloramphenicol	0.19	0.77	0.39	0.19	0.10	0.05	0.10	0.05	0.05	0.77

binuclear Ni(ɪɪ) complex in most cases has higher activity than the mononuclear Cu(ɪɪ) and Zn(ɪɪ) complexes. Bearing in mind these two facts, the reason for the higher antibacterial activity of the bimetallic Mn(ɪɪ) complex can be explained by the existence of two metal centers.

The antifungal activity of the tested compounds is given in Table 3. All tested complexes showed a very good activity towards *A. braziliensi*s and *S. cerevisiae* and the strongest activity against these strains was displayed by binuclear complex **2**. Its activity (MIC 0.09 mM) is comparable to the control compound amphotericin B. All three complexes showed moderate activity against *C. albicans*.

Assessment of toxicity and radical scavenging activity

The obtained toxicity assessment results of the compounds against freshly hatched nauplii *Artemia salina* as well as their radical scavenging activity are given in Table 4. All synthesized

Table 3 Antifungal activity (MIC in mM)

	A. braziliensis	C. albicans	S. cerevisiae
HL^{1}Cl	0.07	0.14	4.48
1	0.30	2.37	0.30
2	0.09	1.44	0.09
3	0.17	0.69	0.17
Cu(BF$_4$)$_2$·6H$_2$O	3.67	7.33	3.67
MnCl$_2$·4H$_2$O	6.32	12.64	6.32
Zn(BF$_4$)$_2$·6H$_2$O	3.60	3.60	3.60
NaN$_3$	0.21	0.42	1.68
Amphotericin B	0.04	0.02	0.01

Table 4 Brine shrimp assay and DPPH radical scavenging activity

	LD50 (mM)	DPPH (mM)
HL^{1}Cl	1.143	0.489
1	0.567	0.094
2	0.315	5.934
3	0.869	31.680
Cu(BF$_4$)$_2$·6H$_2$O	0.312	29.626
MnCl$_2$·4H$_2$O	1.406	—
Zn(BF$_4$)$_2$·6H$_2$O	0.884	—
NaN$_3$	0.537	—
K$_2$Cr$_2$O$_7$	0.077 ± 0.016	
Ascorbic acid	—	0.079 ± 0.018

complexes manifested moderate toxicity, with compound **2** exhibiting the highest toxicity. A possible interpretation of this result could be based on its good antibacterial activity. Since the nauplii live in symbiosis with some bacterial strains, it would be reasonable to assume that complex **2** exhibits its toxicity in this way.

Radical scavenging activity was determined by the DPPH test. Complex **1** showed the best activity. This is in line with the structures of the complexes. The central ion of complex **1** is redox-active Cu^{2+}. The radical scavenging activity of complex **1** is comparable to that of ascorbic acid.

Cytotoxic activities of Cu(ɪɪ) and Mn(ɪɪ) complexes

The cytotoxic activities of the Cu(ɪɪ) complex (**1**), Mn(ɪɪ) complex (**2**), Zn(ɪɪ) complex (**3**) and their precursor compounds against human cancer cell lines and normal keratinocyte cell line are examined and presented in Table 5. All three complexes showed concentration-dependent cytotoxic effects on the tested cell lines. The Cu(ɪɪ) complex (**1**) exerted the highest intensity of cytotoxic activity against melanoma A375, lung carcinoma A549, and prostate adenocarcinoma PC-3 cells with the IC$_{50}$ values of 18.51 µM, 21.35, and 22.73 µM, respectively. The cytotoxicity of this complex was slightly lower against cervical adenocarcinoma HeLa and breast adenocarcinoma MCF7 cells (the IC$_{50}$ values are 28.74 µM and 30.45 µM, respectively). The cytotoxic activity of **1** was similar to that of normal keratinocytes HaCaT with an IC$_{50}$ value of 30.26 µM. The Cu(ɪɪ) complex (**1**) demonstrated stronger cytotoxicity against the A375, A549, and PC-3 cancer cell lines compared to its cytotoxicity against normal HaCaT cells. The highest selectivity of the cytotoxic action of **1** was observed against A375 melanoma cells compared to keratinocytes HaCaT (a selectivity coefficient of 1.63). This complex exhibited notably higher cytotoxic activity against all the tested cell lines compared with the cytotoxic activity of its ligand and precursor compounds (Cu(BF$_4$)$_2$·6H$_2$O and NaN$_3$).

The Mn(ɪɪ) complex (**2**) exerted the strongest cytotoxic effect on breast adenocarcinoma MCF7 cells with an IC$_{50}$ value of 26.66 µM. A moderate cytotoxic activity of this complex was observed against the HeLa, A549, A375, and PC-3 cancer cell lines (IC$_{50}$ values ranging from 40.92 to 52.07 µM). The examined Mn(ɪɪ) complex (**2**) exerted moderate cytotoxicity against

Table 5 Cytotoxic activity of the Cu(II), Mn(II) and Zn(II) complexes and their precursor compounds (IC$_{50}$ [μM] average ± SD)

	HeLa	A375	A549	PC-3	MCF7	HaCaT
HL^{1}Cl	≈200	155.65 ± 5.95	>200	197.67 ± 3.29	199.23 ± 1.09	180.00 ± 4.66
1	28.74 ± 2.93	18.51 ± 2.20	21.35 ± 0.29	22.73 ± 0.52	30.45 ± 3.53	30.26 ± 4.07
2	40.92 ± 1.30	52.07 ± 2.93	44.45 ± 2.66	50.25 ± 0.36	26.66 ± 3.16	41.20 ± 1.70
3	289.10 ± 4.11	292.63 ± 14.65	≈400	362.43 ± 2.96	375.46 ± 10.87	206.92 ± 9.79
NaN$_3$	>200	190.28 ± 13.75	>200	>200	>200	>200
Cu(BF$_4$)$_2$·6H$_2$O	123.14 ± 8.04	110.92 ± 3.25	159.20 ± 4.66	96.98 ± 4.75	99.05 ± 6.86	91.82 ± 1.59
MnCl$_2$·4H$_2$O	48.68 ± 1.25	46.07 ± 5.55	153.86 ± 4.33	118.94 ± 19.10	60.50 ± 3.48	79.56 ± 1.21
Zn(BF$_4$)$_2$·6H$_2$O	171.06 ± 2.85	131.85 ± 11.88	199.22 ± 1.10	192.77 ± 2.63	198.78 ± 1.72	114.15 ± 8.75
Cisplatin	4.00 ± 0.47	2.46 ± 0.34	12.74 ± 1.26	12.29 ± 1.60	17.82 ± 2.58	2.25 ± 0.18

normal keratinocytes HaCaT with an IC$_{50}$ value of 41.20 μM. The selectivity of the cytotoxic activity of this complex was shown only against breast cancer MCF7 cells compared with its activity against the normal cell line (selectivity coefficient of 1.55). The cytotoxic activities of its ligand and precursor compounds NaN$_3$ and MnCl$_2$·4H$_2$O were lower than the activity of **2**. The only exception of this trend was the slightly lower cytotoxicity of the complex **2** against A375 cells compared with the activity of the salt MnCl$_2$·4H$_2$O against A375 cells.

The Cu(II) complex demonstrated stronger cytotoxic effects against tested cancer cell lines than the Mn(II) complex. However, **2** showed selectivity towards breast adenocarcinoma MCF7 cells in contrast to complex **1**. The Zn(II) complex exerted the lowest cytotoxic activity against all the tested cancer cell lines compared to the Cu(II) and Mn(II) complexes including its precursor compounds.

Experimental

Materials and methods

2-Acetylthiazole (99%) was obtained from Acros, Girard's T reagent (99%) from Aldrich, DMSO-d_6 from Merck, methanol from Betahem (Belgrade, Serbia), MnCl$_2$·4H$_2$O from Kemika d. d. (Zagreb, Croatia), NaN$_3$ from Riedel-de Haën, and Cu(BF$_4$)$_2$·6H$_2$O and Zn(BF$_4$)$_2$·6H$_2$O from Sigma-Aldrich. IR spectra were recorded using a Nicolet 6700 FT-IR spectrophotometer using the ATR technique in the region 4000–400 cm^{-1} (vs – very strong, s – strong, m – medium, and w – weak). ^{1}H and ^{13}C NMR spectra were recorded using a Bruker Avance 500 spectrometer (^{1}H at 500 MHz and ^{13}C at 125 MHz) at room temperature using TMS as the internal standard in DMSO-d_6. Chemical shifts are expressed in ppm (δ) values and coupling constants (J) in Hz (splitting patterns: s – singlet and d – doublet). Elemental analyses (C, H, and N) were performed by standard micro-methods using an ELEMENTARVario ELIII C. H.N.S.O analyzer.

Synthesis

Synthesis of *N,N,N*-trimethyl-2-oxo-2-(2-(1-(thiazol-2-yl)ethylidene)hydrazinyl)ethan-1-aminium chloride (HL^{1}Cl) (*E/Z* = 1/1). The ligand **HL^{1}Cl** was synthesized by the reaction of Girard's T reagent and 2-acetylthiazole according to the previously described method.[30]

IR (cm^{-1}): 3387 (w), 3128 (w), 3091 (m), 3017 (m), 2955 (s), 1701 (vs), 1612 (w), 1550 (vs), 1486 (s), 1401 (m), 1300 (w), 1201 (s), 1135 (w), 976 (w), 944 (w), 914 (m), 786 (w), 748 (w), 684 (w), 585 (w), 551 (w). (**HL^{1}Cl-*E***). ^{1}H NMR (500 MHz, DMSO-d_6), δ (ppm): 2.41 (s, 3H, C5–H), 3.30 (s, 9H, C8–H), 4.60 (s, 2H, C7–H), 7.85 (d, 1H, $J_{C2-H/C3-H}$ = 5.0 Hz, C2–H), 7.93 (d, 1H, $J_{C2-H/C3-H}$ = 5.0 Hz, C3–H), 11.61 (s, 1H, N–H). ^{13}C NMR (125 MHz, DMSO-d_6), δ (ppm): 13.90 (C5), 53.65 (C8), 63.01 (C7), 123.33 (C2), 143.94 (C3), 146.98 (C4), 161.23 (C1), 167.04 (C6). (**HL^{1}Cl-*Z***). ^{1}H NMR (500 MHz, DMSO-d_6), δ (ppm): 2.53 (s, 3H, C5–H), 3.34 (s, 9H, C8–H), 4.82 (s, 2H, C7–H), 7.85 (d, 1H, $J_{C2-H/C3-H}$ = 5.0 Hz, C2–H), 7.93 (d, 1H, $J_{C2-H/C3-H}$ = 5.0 Hz, C3–H), 11.86 (s, 1H, N–H). ^{13}C NMR (125 MHz, DMSO-d_6), δ (ppm): 15.05 (C5), 53.89 (C8), 63.76 (C7), 123.65 (C2), 143.97 (C3), 150.80 (C4), 166.78 (C1), 167.34 (C6).

Synthesis of complex [CuL^1(N$_3$)(CH$_3$OH)]BF$_4$ (1). The Cu(II) complex was synthesized by the reaction of **HL^{1}Cl** (70 mg, 0.25 mmol) and Cu(BF$_4$)$_2$·6H$_2$O (86 mg, 0.25 mmol) in methanol (20 mL). After the complete dissolution of Cu(BF$_4$)$_2$·6H$_2$O in the reaction mixture, NaN$_3$ (65 mg, 1 mmol) was added. The mixture was refluxed for 2 h. Green crystals were obtained after slow evaporation of the solvent in a refrigerator (~4 °C) for seven days. Yield: 42 mg (36%). Elemental analysis calcd for C$_{11}$H$_{20}$BCuF$_4$N$_7$O$_2$S: C 28.43%, H 4.34%, N 21.10%, S 6.90%; found: C 28.53%, H 4.15%, N 21.17%, S 6.89%.

IR (cm^{-1}): 3352 (w), 3317 (w), 3077 (m), 3050 (s), 2970 (m), 2940 (w), 2047 (vs), 1829 (w), 1698 (w), 1604 (w), 1522 (s), 1477 (m), 1444 (m), 1413 (m), 1395 (m), 1325 (m), 1287 (m), 1239. (w), 1159 (w), 1124 (w), 1088 (w), 1053 (m), 1007 (m), 961 (w), 939 (w), 917 (m), 878 (w), 783 (m), 735 (w), 656 (w), 631 (w), 563 (w).

Synthesis of complex [Mn$_2$L$^1_2$(μ$_{-1,1}$N$_3$)$_2$(N$_3$)$_2$]·2CH$_3$OH (2). The Mn(II) complex was synthesized by the reaction of **HL^{1}Cl** (70 mg, 0.25 mmol) and MnCl$_2$·4H$_2$O (50 mg, 0.25 mmol) in methanol (20 ml). After complete dissolution of the Mn(II) salt, NaN$_3$ (65 mg, 1 mmol) was added. The mixture was stirred for 2 h at 60 °C. Orange crystals were obtained after slow evaporation of the solvent in a refrigerator (~4 °C) for 14 days. Yield: 50 mg (24%). Elemental analysis calcd for C$_{22}$H$_{40}$Mn$_2$N$_{20}$O$_4$S$_2$: C 32.12%, H 4.90%, N 34.05%, S 7.80%; found: C 31.95%, H 4.87%, N 34.15%, S 7.83%.

IR (cm^{-1}): 3388 (s), 3086 (m), 3036 (m), 2111 (w), 2042 (vs), 1688 (w), 1643 (w), 1595 (w), 1533 (s), 1481 (s), 1425 (m), 1331 (m), 1273 (m), 1202 (w), 1136 (w), 1115 (w), 1062 (w), 1043 (w), 1004 (w), 928 (w), 907 (w), 879 (w), 768 (w), 723 (w), 640 (w).

Synthesis of complex [ZnL¹(N₃)₂] (3). The Zn(II) complex was synthesized by the reaction of **HL¹Cl** (70 mg, 0.25 mmol) and Zn(BF₄)₂·6H₂O (86 mg, 0.25 mmol) in methanol (20 ml). After the complete dissolution of Zn(BF₄)₂·6H₂O in the reaction mixture, NaN₃ (65 mg, 1 mmol) was added. The mixture was refluxed for 2 h and filtered. Yellow crystals were obtained after slow evaporation of the solvent in a refrigerator (~4 °C) for seven days. Yield: 40 mg (41%). Elemental analysis calcd for $C_{10}H_{16}N_{10}OSZn$: C 30.82%, H 4.14%, N 35.94%, S 8.23%; found: C 30.76%, H 4.18%, N 35.83%, S 8.21%.

IR (cm⁻¹): 3378 (w), 3078 (w), 3054 (w), 3009 (w), 2964 (w), 2057 (vs), 1600 (w), 1540 (s), 1481 (w), 1433 (w), 1407 (w), 1339 (m), 1285 (w), 1203 (w), 1153 (w), 1116 (w), 1079 (w), 1057 (w), 1009 (w), 975 (w), 971 (w), 880 (w), 738 (w), 642 (w). ¹H NMR (500 MHz, DMSO-d_6), δ (ppm): 2.53 (s, 3H, C5–H), 3.23 (s, 9H, C8–H), 4.13 (s, 2H, C7–H), 7.92 (d, 1H, $J_{C2-H/C3-H}$ = 5.0 Hz, C2–H), 8.04 (d, 1H, $J_{C2-H/C3-H}$ = 5.0 Hz, C3–H). ¹³C NMR (125 MHz, DMSO-d_6), δ (ppm): 15.73 (C5), 53.96 (C8), 67.11 (C7), 124.82 (C2), 143.44 (C3), 147.32 (C4), 165.93 (C1), 171.59 (C6).

X-ray crystallography

Crystal data and the refinement parameters of compounds **1–3** are listed in Table 6. Single crystal X-ray diffraction data were collected at room temperature using an Agilent SuperNova dual-source diffractometer with an Atlas detector equipped with mirror-monochromated Mo–K$_\alpha$ radiation (λ = 0.71073 Å). Data processing was performed with CrysAlis PRO.[43] The structures were solved with Olex software[44] using SHELXT[45] or SHELXS[46] and refined by a full-matrix least-squares based on F^2 using SHELXL.[47] All non-hydrogen atoms were refined anisotropically. All other hydrogen atoms were included in the model at geometrically calculated positions and refined using a riding model. The ORTEP-3[48] for Windows and MERCURY[49] programs were used for graphical presentations. Crystallographic data for complexes **1–3** have been deposited with the Cambridge Crystallographic Data Centre as CCDC 2110386–2110388.†

Computational details

All DFT calculations were done with the ADF program package (version 2017).[50–52] Relativistic effects were accounted for by the scalar-relativistic Zeroth-Order Regular Approximation (ZORA).[53–55] The all-electron triple-zeta Slater-type orbitals plus one polarization function (TZP) basis set was used for all atoms. All open-shell systems are treated with unrestricted formalism in their high-spin state. The COSMO solvation model,[56,57] as implemented in ADF,[58] with DMSO as the solvent was used. Geometry optimizations were performed using general gradient functional consisting of Becke's exchange[59] and Perdew's correlation[60] with Grimme's third-generation dispersion energy correction[61] and Becke–Johnson damping,[62] *i.e.*, BP86-D3. The Cartesian coordinates of all the optimized structures are available in the ESI.† Analytical harmonic frequencies[63–65] were calculated at the same level of theory. All normal modes with small frequencies (<50 cm⁻¹) were rescanned numerically[66,67] to ascertain that all the optimized structures correspond to the minima on the potential energy surface. Vibrational analysis in the quasi-harmonic

Table 6 Crystal data and structure refinement details for **1**, **2** and **3**

	1	2	3
Formula	$C_{11}H_{20}BCuF_4N_7O_2S$	$C_{22}H_{40}Mn_2N_{20}O_4S_2$	$C_{10}H_{16}N_{10}OSZn$
F_w (g mol⁻¹)	464.75	822.74	389.76
Crystal size (mm)	0.60 × 0.60 × 0.20	0.40 × 0.40 × 0.20	0.60 × 0.30 × 0.20
Crystal color	Green	Orange	Yellow
Crystal system	Monoclinic	Triclinic	Monoclinic
Space group	$P2_1/n$	$P\bar{1}$	$P2_1/c$
a (Å)	7.0033(3)	9.6427(5)	13.0826(10)
b (Å)	10.8941(3)	10.8396(5)	10.2506(7)
c (Å)	25.6059(9)	10.8617(8)	13.1685(13)
α(°)	90	106.971(5)	90
β (°)	97.242(4)	103.497(5)	111.237(10)
γ(°)	90	112.469(5)	90
V (Å³)	1938.01(12)	923.85(10)	1646.0(3)
Z	4	1	4
Calcd density (g cm⁻³)	1.593	1.479	1.573
F(000)	948	426	800
No. of collected reflns	17 559	10 077	13 910
No. of independent reflns	4425	4144	3779
R_{int}	0.0235	0.0311	0.0315
No. of reflns observed	3789	3319	2489
No. parameters	287	232	212
$R[I > 2\sigma (I)]^a$	0.0388	0.0371	0.0481
wR_2(all data)^b	0.1110	0.0982	0.1230
Goof, S^c	1.157	1.072	1.084
Maximum/minimum residual electron density (e Å⁻³)	+0.48/−0.34	+0.28/−0.31	+0.63/−0.77

^{a} $R = \sum||F_o| - |F_c||/\sum|F_o|$. ^{b} $wR_2 = \{\sum[w(F_o^2 - F_c^2)^2]/\sum[w(F_o^2)^2]\}^{1/2}$. ^{c} $S = \{\sum[(F_o^2 - F_c^2)^2]/(n/p)\}^{1/2}$ where n is the number of reflections and p is the total number of parameters refined.

approximation as proposed by Truhlar[68,69] (frequency cut-off 100 cm^{-1}) was used to evaluate the zero-point effects and the entropic and thermal corrections to the Gibbs free energy at 298 K. Because vibrational analysis is done at a standard state of 1 atm, a conversion to 1 mol dm^{-3} solution standard state is done. This gives a correction of 1.89 kcal mol^{-1} to the free energies (at 298 K). This correction is important only for reactions where the number of moles changes. In reactions where DMSO is involved, the free energy correction due to the conversion to the solvent standard state (13.98 mol dm^{-3}) equals 3.46 kcal mol^{-1} (at 298 K). Entropy correction due to spin-multiplicity ($R \ln(g_s)$, where g_s is the spin-degeneracy of a complex and R is the universal gas constant) was employed. When binuclear $[Mn_2L^1_2(\mu_{-1,1}\text{-}N_3)_2(N_3)_2]$ is considered, the low-lying excited states due to the exchange coupling are included in thermochemical analysis. Electronic energies used to calculate the Gibbs free energy were evaluated with the M06-2X[70,71] meta-hybrid functional, at ZORA-BP86-D3/TZP-COSMO(DMSO) geometries. The Lib$_{XC}$ library[72] was used for M06-2X calculations. Free energy changes for each considered reaction were corrected for the basis set superposition error by the fragment approach and "ghost atoms" in ADF. The exchange coupling constant J in $[Mn_2L^1_2(\mu_{-1,1}\text{-}N_3)_2(N_3)_2]$ was calculated with broken-symmetry DFT formalism[73–77] at the ZORA-M06-2X/TZP level of theory at X-ray and ZORA-BP86-D3/TZP-COSMO(DMSO) geometries according to the Yamaguchi approach.[78] Broken symmetry solutions are obtained from the high-spin states using the spin–flip method. The calculated exchange coupling constants were used to estimate the relative energies of the low-lying spin-states through diagonalization of the spin Hamiltonian ($H = -2JS_1S_2$).

Antimicrobial activity

Antimicrobial activity was tested against a panel of microorganisms including Gram-negative bacteria *Escherichia coli* (ATCC 25922), *Pseudomonas aeruginosa* (ATCC 9027), *Proteus hauseri* (ATCC 13315), *Klebsiella pneumoniae* (ATCC 10031), and *Salmonella enterica* subsp. *enterica* serovar Enteritidis (ATCC 13076), Gram-positive bacteria *Staphylococcus aureus* (ATCC 6538), *Bacillus spizizenii* (ATCC 6633), *Clostridium sporogenes* (ATCC 19404), *Micrococcus luteus* (ATCC 4698), and *Micrococcus luteus* (ATCC 10240), yeasts *Candida albicans* (ATCC 10231) and *Saccharomyces cerevisiae* (ATCC 9763) and fungal strain *Aspergillus brasiliensis* (ATCC 16404).

Antimicrobial activity was evaluated using the broth microdilution method according to NCCLS [National Committee for Clinical Laboratory Standards, Approval Standard Document M7-A5, Villanova, PA, USA, 2000]. The 96-well plates were prepared by dispensing 100 µl of Mueller–Hinton broth for bacteria and the Sabouraud dextrose broth for yeasts and fungi into each well. A 100 µL aliquot from the stock solution of the tested compounds (concentration 10 mg mL^{-1} in DMSO) was added into the first row of the plate and double diluted by using a multichannel pipette. The direct colony method was used in the preparation of a suspension of bacteria and yeasts in sterile 0.9% saline, while the process of preparing the suspension of fungal spores included gentle stripping of spores from agar slants with growing aspergilli into sterile 0.9% saline. Suspension turbidity evaluation was conducted by comparison with 0.5 McFarland's standard. 10 µL of diluted bacterial, yeast or spore suspension was added to each well to give a final concentration of 5×10^5 CFU mL^{-1} for bacteria and 5×10^3 CFU mL^{-1} for fungi and yeast. Chloramphenicol served as a positive control for bacteria, while amphotericin B served as a positive control for yeasts and fungi.

The inoculated plates were incubated at 37 °C for 24 h for bacteria and at 28 °C for 48 h for the yeasts and fungi. The bacterial growth was visualized by adding 20 µL of 0.5% 2,3,5-triphenyltetrazolium chloride (TTC) aqueous solution.[79] Minimum inhibitory concentration (MIC) was defined as the lowest concentration of the compounds that inhibited bacterial growth (red-colored pellet at the bottom of the wells after the addition of TTC).

Brine shrimp assay

About 20 g of commercially purchased lyophilized eggs of *Artemia salina* was added to 0.5 L of tap water, and air was passed through the suspension by a pump under illumination for 48 h. All tested compounds were dissolved in DMSO and various amounts (0.01–1 mg) were added to 950 µL of artificial seawater with freshly hatched nauplii. After 24 h illumination at room temperature, the number of dead and surviving nauplii were counted and statistically analyzed. LC$_{50}$ was defined as a concentration of compounds that caused the death of 50% of the nauplii. All samples were done in triplicate.

DPPH radical scavenging activity

The 2,2-diphenyl-1-picrylhydrazyl (DPPH) radical scavenging activity was determined by the method of Blois.[80] Commercially available free radical DPPH was dissolved in methanol at a concentration of 6.58×10^{-5} M, while the tested compounds were dissolved in DMSO. Into a 96-well microplate, 50 µL solutions of the tested compounds at concentrations ranging from 10 to 0.02 mg mL^{-1} were loaded (50 µL DMSO in the control) and 100 µL of DPPH solution were added. After incubation for 30 min at room temperature in the dark, the absorbance was measured at 517 nm. All the measurements were performed in triplicate and the scavenging activity of the tested derivatives was calculated as

$$\text{Scavenging activity } (\%) = 100 \times (A_{control} - (A_{sample} - A_0))/A_{control}$$

where $A_{control}$ and A_{sample} refer to the absorbance of DPPH in the control solution and sample, respectively, while A_0 refers to the absorbance of the solutions of compounds, because of their color.

The IC$_{50}$ value was defined as the antioxidant concentration necessary to decrease the amount of the initial DPPH radical by 50% and was calculated from the plotted graph of scavenging activities against the concentrations of the tested com-

pounds. Ascorbic acid was employed as the positive control (concentrations ranging from 50 to 500 µg mL^{-1}).

Determination of cytotoxic activity

The cytotoxic activity of the newly synthesized Cu(II) and Mn(II) complexes and their precursor compounds was examined on five human cancer cell lines: cervical adenocarcinoma HeLa, melanoma A375, lung carcinoma A549, prostate adenocarcinoma PC-3, and breast adenocarcinoma MCF7, as well as against normal human keratinocyte cell line HaCaT. Stock solutions of the compounds were made in DMSO at a concentration of 10 mM, with the exception of the stock solution of Cu(II)complex, which was made at a concentration of 7.5 mM. The human cell lines were grown in a complete nutrient medium RPMI-1640 supplemented with 10% fetal bovine serum, 2 mM L-glutamine, and penicillin–streptomycin solution. HeLa (3000 cells per well), A375 (3000 cells per well), A549 (5000 cells per well), MCF7 (7000 cells per well), PC-3 (5000 cells per well), and HaCaT cells (7000 cells per well) were seeded in 96-well microtiter plates and after 20 h the cells were treated with two complexes and their precursor compounds (five increasing concentrations were tested, ranging from 12.5 µM–200 µM). The nutrient medium was added only to control cells. After 72 h treatment, cell survival was determined by MTT assay according to the method firstly described by Mosmann,[81] and modified by Ohno and Abe[82] and described in more detail elsewhere.[83] Each of the three independent experiments was performed in triplicate. A chemotherapeutic drug, cisplatin, was used as a positive control.

Conclusions

Complexes **1–3** have been synthesized and characterized by X-ray crystallographic analysis, elemental analysis and IR spectroscopy. NMR spectroscopy results for the Zn(II) complex showed its stability in solution. The hydrazone ligand is coordinated in a deprotonated form in all three complexes through the thiazole nitrogen, azomethine nitrogen, and carbonyl oxygen atoms. The five-coordination geometry of the Cu(II) ion (mononuclear complex **1**) can be described as distorted square-based pyramidal, while in the case of the Zn(II) ion (mononuclear complex **3**), the geometry is somewhere in-between square-based pyramidal and trigonal bipyramidal form. The geometry around the Mn(II) ion (binuclear complex **2**) is distorted trigonal prism with three donor atoms from the hydrazone ligand, two nitrogen atoms from bridging azide anions, and one nitrogen atom from the terminal azide anion. According to the DFT studies, the Cu(II) complex is the most stable in square-planar [CuL^1(N$_3$)]$^+$ geometry in DMSO solution, while in the same solution a mixture of pentacoordinate [MnL^1(N$_3$)$_2$] and binuclear Mn(II) complex is predicted.

The novel Cu(II) complex showed pronounced cytotoxic effects against tested human cancer cell lines. The complex exerted a higher intensity of cytotoxic activity against A375, A549, and PC-3 cancer cells compared to the intensity of cyto-

toxicity against normal keratinocytes HaCaT. In addition, the novel Mn(II) complex demonstrated potent cytotoxicity against MCF7 cells. Moderate cytotoxic activity of this complex was observed against other tested cancer cell lines. In general, the Cu(II) complex exhibits more potent cytotoxicity than the Mn(II) complex. However, the activity of complex **2** against the MCF7 breast cancer cell line is very promising as it is only slightly weaker than the activity of cisplatin. However, in contrast to cisplatin, it is selective to the tumor cell line in comparison with the normal cell line (HaCaT).

Conflicts of interest

There are no conflicts to declare.

Acknowledgements

References

1 M. N. Uddin, S. S. Ahmed and S. M. R. Alam, *J. Coord. Chem.*, 2020, **73**, 3109–3149.

2 M. R. Milenković, B. Čobeljić, K. Anđelković and I. Turel, *Eur. J. Inorg. Chem.*, 2018, **2018**, 838–846.

3 D. Krajčiová, M. Melník, E. Havránek, A. Forgácsová and P. Mikuš, *J. Coord. Chem.*, 2014, **67**, 1493–1519.

4 R. C. Balachandran, S. Mukhopadhyay, D. McBride, J. Veevers, F. E. Harrison, M. Aschner, E. N. Haynes and A. B. Bowman, *J. Biol. Chem.*, 2020, **295**, 6312–6329.

5 D. S. Auld, *BioMetals*, 2001, **14**, 271–313.

6 M. Stojičkov, S. Sturm, B. Čobeljić, A. Pevec, M. Jevtović, A. Scheitler, D. Radanović, L. Senft, I. Turel, K. Andjelković, M. Miehlich, K. Meyer and I. Ivanović-Burmazović, *Eur. J. Inorg. Chem.*, 2020, **2020**, 3347–3358.

7 O. Iranzo, *Bioorg. Chem.*, 2011, **39**, 73–87.

8 S. Karabasannavar, P. R. Allolli and B. M. Kalshetty, *Indian J. Pharm. Educ. Res.*, 2017, **51**, 748–757.

9 M. M. E. Shakdofa, F. A. El-Saied, A. J. Rasras and A. N. Al-Hakimi, *Appl. Organomet. Chem.*, 2018, **32**, 4376–4393.

10 S. M. Emam, S. A. Abouel-Enein and E. M. Abdel-Satar, *Appl. Organomet. Chem.*, 2019, **33**, 4847–4872.

11 S. M. H. Obaid, J. S. Sultan and A. A. S. Al-Hamdani, *Indones. J. Chem.*, 2020, **20**, 1311–1322.

12 B. Shaabani, A. A. Khandar, N. Ramazani, M. Fleck, H. Mobaiyen and L. Cunha-Silva, *J. Coord. Chem.*, 2017, **70**, 696–708.

13 P. Jain, D. Kumar, S. Chandra and N. Misra, *Appl. Organomet. Chem.*, 2020, **34**, e5371.

14 L.-W. Xue, X. Fu, G.-Q. Zhao and Q.-B. Li, *Acta Chim. Slov.*, 2021, **68**, 17–24.

15 L.-H. Wang, X.-Y. Qiu and S.-J. Liu, *J. Coord. Chem.*, 2019, **72**, 962–971.

16 N. Biswas, S. Saha, S. Khanra, A. Sarkar, D. Mandal, S. Bhattacharjee, A. Chaudhuri, S. Chakraborty and C. R. Choudhury, *J. Biomol. Struct. Dyn.*, 2019, **37**, 2801–2822.

17 A. Mondal, C. Das, M. Corbella, A. Bauzá, A. Frontera, M. Saha, S. Mondal, K. das Saha and S. K. Chattopadhyay, *New J. Chem.*, 2020, **44**, 7319–7328.

18 E. Ramachandran, V. Gandin, R. Bertani, P. Sgarbossa, K. Natarajan, N. S. P. Bhuvanesh, A. Venzo, A. Zoleo, A. Glisenti, A. Dolmella, A. Albinati and C. Marzano, *J. Inorg. Biochem.*, 2018, **182**, 18–28.

19 Y.-F. Chen, L. Wei, J.-L. Bai, H. Zhou, Q.-M. Huang, J.-B. Li and Z.-Q. Pan, *J. Coord. Chem.*, 2011, **64**, 1153–1164.

20 S. Y. Ebrahimipour, M. Mohamadi, J. Castro, N. Mollania, H. A. Rudbari and A. Saccá, *J. Coord. Chem.*, 2015, **68**, 632–649.

21 A. Th. Chaviara, P. J. Cox, K. H. Repana, A. A. Pantazaki, K. T. Papazisis, A. H. Kortsaris, D. A. Kyriakidis, G. St Nikolov and C. A. Bolos, *J. Inorg. Biochem.*, 2005, **99**, 467–476.

22 J.-A. Zhang, Y. Li, Y.-Z. Fan, X.-Z. Zou, Y.-J. Liu, L.-J. Zhang and S.-R. Zheng, *Inorg. Chem. Commun.*, 2014, **49**, 136–139.

23 H. A. EL-Ghamry, K. Sakai, S. Masaoka, K. Y. El-Baradie and R. M. Issa, *Chin. J. Chem.*, 2012, **30**, 881–890.

24 Y. M. Ahmed, W. H. Mahmoud, M. M. Omar and G. G. Mohamed, *J. Inorg. Organomet. Polym. Mater.*, 2021, **31**, 2339–2359.

25 B. Čobeljić, I. Turel, A. Pevec, Z. Jagličić, D. Radanović, K. Anđelković and M. R. Milenković, *Polyhedron*, 2018, **155**, 425–432.

26 M. Č. Romanović, B. Čobeljić, A. Pevec, I. Turel, S. Grubišić, D. Radanović, K. Anđelković, M. Milenković and M. R. Milenković, *J. Coord. Chem.*, 2017, **70**, 3702–3714.

27 K. Anđelković, M. R. Milenković, A. Pevec, I. Turel, I. Z. Matić, M. Vujčić, D. Sladić, D. Radanović, G. Brađan, S. Belošević and B. Čobeljić, *J. Inorg. Biochem.*, 2017, **174**, 137–149.

28 G. Brađan, A. Pevec, I. Turel, I. N. Shcherbakov, M. Milenković, M. Milenković, D. Radanović, B. Čobeljić and K. Anđelković, *J. Coord. Chem.*, 2016, **69**, 2754–2765.

29 G. Brađan, B. Čobeljić, A. Pevec, I. Turel, M. Milenković, D. Radanović, M. Šumar-Ristović, K. Adaila, M. Milenković and K. Anđelković, *J. Coord. Chem.*, 2016, **69**, 801–811.

30 T. T. Adejumo, N. V. Tzouras, L. P. Zorba, D. Radanović, A. Pevec, S. Grubišić, D. Mitić, K. K. Anđelković, G. C. Vougioukalakis, B. Čobeljić and I. Turel, *Molecules*, 2020, **25**, 4043–4060.

31 K. Nakamoto, *Infrared and Raman Spectra of Inorganic and Coordination Compounds*, Wiley-Interscience, New York, 4th edn, 1986.

32 A. W. Addison, T. N. Rao, J. Reedijk, J. van Rijn and G. C. Verschoor, *J. Chem. Soc., Dalton Trans.*, 1984, 1349–1356.

33 T. Keškić, B. Čobeljić, M. Gruden, K. Anđelković, A. Pevec, I. Turel, D. Radanović and M. Zlatar, *Cryst. Growth Des.*, 2019, **19**, 4810–4821.

34 M. R. Milenković, A. T. Papastavrou, D. Radanović, A. Pevec, Z. Jagličić, M. Zlatar, M. Gruden, G. C. Vougioukalakis, I. Turel, K. Anđelković and B. Čobeljić, *Polyhedron*, 2019, **165**, 22–30.

35 T. Keškić, B. Čobeljić, M. Gruden, K. Anđelković, A. Pevec, I. Turel, D. Radanović and M. Zlatar, *Cryst. Growth Des.*, 2019, **19**, 4810–4821.

36 K. R. Dymock and G. J. Palenik, *Inorg. Chem.*, 1975, **14**, 1220–1222.

37 T. Keškić, Z. Jagličić, A. Pevec, B. Čobeljić, D. Radanović, M. Gruden, I. Turel, K. Anđelković, I. Brčeski and M. Zlatar, *Polyhedron*, 2020, **191**, 114802–114814.

38 T. Steiner, *Angew. Chem., Int. Ed.*, 2002, **41**, 48–76.

39 B. Čobeljić, A. Pevec, S. Stepanović, M. R. Milenković, I. Turel, M. Gruden, D. Radanović and K. Anđelković, *Struct. Chem.*, 2018, **29**, 1797–1806.

40 K. Anđelković, A. Pevec, S. Grubišić, I. Turel, B. Čobeljić, M. R. Milenković, T. Keškić and D. Radanović, *J. Mol. Struct.*, 2018, **1162**, 63–70.

41 M. Č. Romanović, B. Čobeljić, A. Pevec, I. Turel, K. Anđelković, M. Milenković, D. Radanović, S. Belošević and M. R. Milenković, *J. Coord. Chem.*, 2017, **70**, 2425–2435.

42 N. Stevanović, P. P. Mazzeo, A. Bacchi, I. Z. Matić, M. Đordić Crnogorac, T. Stanojković, M. Vujčić, I. Novaković, D. Radanović, M. Šumar-Ristović, D. Sladić, B. Čobeljić and K. Anđelković, *JBIC, J. Biol. Inorg. Chem.*, DOI: 10.1007/s00775-021-01893-5.

43 Agilent, 2014.

44 O. V. Dolomanov, L. J. Bourhis, R. J. Gildea, J. A. K. Howard and H. Puschmann, *J. Appl. Crystallogr.*, 2009, **42**, 339–341.

45 G. M. Sheldrick, *Acta Crystallogr., Sect. A: Found. Adv.*, 2015, **71**, 3–8.

46 G. M. Sheldrick, *Acta Crystallogr., Sect. A: Found. Crystallogr.*, 2008, **64**, 112–122.

47 G. M. Sheldrick, *Acta Crystallogr., Sect. C: Struct. Chem.*, 2015, **71**, 3–8.

48 L. J. Farrugia, *J. Appl. Crystallogr.*, 2012, **45**, 849–854.

49 C. F. Macrae, P. R. Edgington, P. McCabe, E. Pidcock, G. P. Shields, R. Taylor, M. Towler and J. van de Streek, *J. Appl. Crystallogr.*, 2006, **39**, 453–457.

50 E. J. Baerends, J. Autschbach, D. Bashford, A. Bérces, F. M. Bickelhaupt, C. Bo, P. M. Boerrigter, L. Cavallo, D. P. Chong, L. Deng, R. M. Dickson, D. E. Ellis, M. van Faassen, L. Fan, T. H. Fischer, C. F. Guerra, A. Ghysels, A. Giammona, S. J. A. van Gisbergen, A. W. Götz, J. A. Groeneveld, O. V. Gritsenko, M. Groening, F. E. Harris, P. van den Hoek, C. R. Jacob, H. Jacobsen, L. Jensen, G. van Kessel, F. Kootstra, M. V. Krykunov, E. van Lenthe, D. A. McCormack, A. Michalak, M. Mitoraj, J. Neugebauer,

V. P. Nicu, L. Noodleman, V. P. Osinga, S. Patchkovskii, P. H. T. Philipsen, D. Post, C. C. Pye, W. Ravenek, J. I. Rodriguez, P. Ros, P. R. T. Schipper, G. Schreckenbach, M. Seth, J. G. Snijders, M. Sola, M. Swart, D. Swerhone, G. te Velde, P. Vernooijs, L. Versluis, L. Visscher, O. Visser, F. Wang, T. A. Wesolowski, E. M. van Wezenbeek, G. Wiesenekker, S. K. Wolff, T. K. Woo, A. L. Yakovlev and T. Ziegler.

51 G. te Velde, F. M. Bickelhaupt, E. J. Baerends, C. F. Guerra, S. J. A. van Gisbergen, J. G. Snijders and T. Ziegler, *J. Comput. Chem.*, 2001, **22**, 931–967.

52 C. F. Guerra, J. G. Snijders, G. te Velde and E. J. Baerends, *Theor. Chem. Acc.*, 1998, **99**, 391–403.

53 E. van Lenthe, E. J. Baerends and J. G. Snijders, *J. Chem. Phys.*, 1993, **99**, 4597–4610.

54 E. van Lenthe, E. J. Baerends and J. G. Snijders, *J. Chem. Phys.*, 1994, **101**, 9783–9792.

55 C. van Wüllen and C. van Wüllen, *J. Chem. Phys.*, 1998, **109**, 392–399.

56 A. Klamt and G. Schoermann, *J. Chem. Soc., Perkin Trans. 2*, 1993, 799–805.

57 A. Klamt, *J. Phys. Chem.*, 1995, **99**, 2224–2235.

58 C. C. Pye and T. Ziegler, *Theor. Chem. Acc.*, 1999, **101**, 396–408.

59 A. D. Becke, *Phys. Rev. A*, 1988, **38**, 3098–3100.

60 J. P. Perdew, *Phys. Rev. B: Condens. Matter Mater. Phys.*, 1986, **33**, 8822–8824.

61 S. Grimme, J. Antony, S. Ehrlich and H. Krieg, *J. Chem. Phys.*, 2010, **132**, 154104.

62 S. Grimme, S. Ehrlich and L. Goerigk, *J. Comput. Chem.*, 2011, **32**, 1456–1465.

63 A. Bérces, R. M. Dickson, L. Fan, H. Jacobsen, D. Swerhone, T. Ziegler, A. Brces, R. M. Dickson, L. Fan, H. Jacobsen, D. Swerhone and T. Ziegler, *Comput. Phys. Commun.*, 1997, **100**, 247–262.

64 H. Jacobsen, A. Bérces, D. P. Swerhone, T. Ziegler, A. Brces, D. P. Swerhone and T. Ziegler, *Comput. Phys. Commun.*, 1997, **100**, 263–276.

65 S. K. Wolff, *Int. J. Quantum Chem.*, 2005, **104**, 645–659.

66 L. Fan and T. Ziegler, *J. Chem. Phys.*, 1992, **96**, 9005–9012.

67 L. Fan and T. Ziegler, *J. Am. Chem. Soc.*, 1992, **114**, 10890–10897.

68 Y. Zhao and D. G. Truhlar, *Phys. Chem. Chem. Phys.*, 2008, **10**, 2813–2818.

69 R. F. Ribeiro, A. V. Marenich, C. J. Cramer and D. G. Truhlar, *J. Phys. Chem. B*, 2011, **115**, 14556–14562.

70 Y. Zhao and D. G. Truhlar, *J. Chem. Phys.*, 2006, **125**, 194101.

71 Y. Zhao and D. G. Truhlar, *Theor. Chem. Acc.*, 2008, **120**, 215–241.

72 M. A. L. Marques, M. J. T. Oliveira and T. Burnus, *Comput. Phys. Commun.*, 2012, **183**, 2272–2281.

73 G. Jonkers, C. A. de Lange, L. Noodleman and E. J. Baerends, *Mol. Phys.*, 1982, **46**, 609–620.

74 L. Noodleman, *J. Chem. Phys.*, 1981, **74**, 5737–5743.

75 L. Noodleman and E. R. Davidson, *Chem. Phys.*, 1986, **109**, 131–143.

76 L. Noodleman, J. G. Norman, J. H. Osborne, A. Aizman and D. A. Case, *J. Am. Chem. Soc.*, 1985, **107**, 3418–3426.

77 F. Neese, *Coord. Chem. Rev.*, 2009, **253**, 526–563.

78 T. Soda, Y. Kitagawa, T. Onishi, Y. Takano, Y. Shigeta, H. Nagao, Y. Yoshioka and K. Yamaguchi, *Chem. Phys. Lett.*, 2000, **319**, 223–230.

79 A. Sartoratto, A. L. M. Machado, C. Delarmelina, G. M. Figueira, M. C. T. Duarte and V. L. G. Rehder, *Braz. J. Microbiol.*, 2004, **35**, 275–280.

80 M. S. Blois, *Nature*, 1958, **181**, 1199–1200.

81 T. Mosmann, *J. Immunol. Methods*, 1983, **65**, 55–63.

82 M. Ohno and T. Abe, *J. Immunol. Methods*, 1991, **145**, 199–203.

83 I. Z. Matić, I. Aljančić, Ž. Žižak, V. Vajs, M. Jadranin, S. Milosavljević and Z. D. Juranić, *BMC Complementary Altern. Med.*, 2013, **13**, 36–48.